Research Article/Mechanical, Mechatronics, and Materials Engineering http://doi.org/10.15446/ing.investig.105266

Experimental Study of Innovative FRC Dome-Shaped Structures with Industrial, Recycled, and Alternative Reinforcing under Compressive Load

Estudio experimental de estructuras innovadoras en forma de cúpula de FRC con refuerzo industrial, reciclado y alternativo bajo cargas de compresión

Alejandro Meza-de Luna[1], Elia Mercedes Alonso-Guzman[2], and Adrián Bonilla-Petriciolet[3]

ABSTRACT

Arc concrete structures are aesthetic and suitable for buildings with large spans. Within the framework of this research, fiber-reinforced concrete (FRC) dome-shaped structures were studied in a lab, analyzing mechanical performance via strength, deformation, and failure mode. The studied FRC was elaborated with industrial, recycled, and alternative fibers. The mold used for producing the dome specimens was made up of two parts in order to favor extraction. This study considered 21 dome samples reinforced with fibers and one control, with replication for those with atypical behavior. The results show that the load-displacement behavior of dome-shaped elements increases with the incorporation of fibers, which depends on the fiber dose and the material. Moreover, the efficiency analysis proved that specimens with low fiber content (20 and 2 kg/m^3) have the best strength-reinforcement relation. The recycled and alternative fibers exhibit good mechanical performance and ductility. The main contribution of this research is a study of the scope and limitations of different types of FRC as the only reinforcement in arched structures.

Keywords: fiber-reinforced concrete, thick-walled shell, dome-shaped structures, experimental research, mechanical behavior, alternative and recycled materials

RESUMEN

Las estructuras de concreto en arco son estéticas y adecuadas para edificios de grandes claros. En el marco de esta investigación se estudiaron las estructuras en forma de domo de concreto reforzado con fibra (FRC) en un laboratorio, analizando el rendimiento mecánico a través de la resistencia, la deformación y el modo de falla. Los FRC estudiados fueron elaborados con fibras industriales, recicladas y alternativas. El molde utilizado para elaborar los especímenes de cúpula estuvo compuesto de dos secciones para favorecer la extracción. Este estudio consideró 21 muestras de domos reforzados con fibras y un control, con replicación sobre aquellas que presentaron un comportamiento atípico. Los resultados muestran que el comportamiento carga-desplazamiento de los elementos en forma de cúpula aumenta con la incorporación de fibras, lo cual depende de la dosis de fibra y el material. Además, el análisis de eficiencia demostró que las muestras con bajo contenido de fibra (20 y 2 kg/m^3) tienen la mejor relación resistencia-refuerzo. Las fibras recicladas y alternativas presentan buen desempeño mecánico y ductilidad. La principal contribución de esta investigación es el estudio de los alcances y limitaciones de diferentes tipos de FRC como único refuerzo en estructuras arqueadas.

Palabras clave: concreto reforzado con fibra, cascarón de paredes gruesas, estructuras en forma de cúpula, investigación experimental, comportamiento mecánico, materiales alternativos y reciclados

Received: October 13th, 2022
Accepted: August 17th, 2023

Introduction

Concrete is a material with high compressive strength. However, it is a ceramic material, so it exhibits brittle failure with low resistance under tensile load, which produces cracking and structural failures (Abhishek and Arabinda, 2020; Abbood *et al*., 2020). This composite material has been the basis for complex structures, complying with the architectural ideas of different designers, such as the Felix Candelas hyperbolic-paraboloid structures (Pereira, 2018). Researchers have proven that curved structures have a high compressive strength. Usually, this shape is seen in sports stadiums, exhibition centers, transport terminals, airports, and religious precincts, highlighting their elegance and strength-weight relationship (Wenfeng *et al*., 2019; Cocchetti *et al*., 2011; Gomes *et al*., 2018; Tomás *et al*., 2010; Caycedo *et al*., 2019).

[1] Mechanical engineer, PhD, Affiliation: Professor, Tecnológico Nacional de México/IT de Aguascalientes, México. E-mail: alejandro.meza@mail.ita.mx
[2] Civil engineer, PhD, Affiliation: Professor, FIC, Universidad Michoacana de San Nicolas de Hidalgo, México. E-mail: elia.alonso@umich.mx
[3] Chemical engineer, PhD, Affiliation: Tecnológico Nacional de México/IT Aguascalientes, México. E-mail: petriciolet@hotmail.com

A shell element is a curved structure with a wall thickness smaller than the diameter and height. It is classified into two branches: thin-shell and thick-shell (Berger *et al*., 2020a; Berger *et al*., 2020b). These structures are generally studied using two strategies: analysis by computer and full-scale experimentation. Caycedo *et al*. (2019), Verwimp *et al*. (2016), and Zingoni *et al*. (2013) evaluated the capacity of thin-walled shell elements using finite element analysis. Their results proved that these structural concrete elements have great plastic strain and buckling load, where the mechanical behavior depends on the structure geometry. Based on experimentation on thin shells with a span of 3 m, Du *et al*. (2019) highlighted the importance of the arc on the mechanical performance of concrete shell elements. Sharei *et al*. (2017) studied the structural performance of concrete shells reinforced with textile material, finding a good agreement between experimental and analytical studies. In addition, analytical studies have been conducted to understand the mechanical performance of concrete shell elements. Tamayo *et al*. (2013) and Chun (2005) analyzed the strength of concrete shell structures, and their results showed an approximation between the proposed mathematical model and the experimental data.

On the other hand, the search for light concrete structures with quick reinforcing has promoted the development of fiber-reinforced concrete (FRC). FRC is a composite material of cement, water, and aggregates reinforced with randomly distributed discrete elements. Fibers are used to enhance the mechanical performance of the concrete matrix, as they have a superior tensile strength to the base material (Meza *et al*., 2021; Daud *et al*., 2020; Meza and Shaikh, 2020; Meza and Siddique, 2019; Chiaia *et al*., 2009; Cadoni *et al*., 2009; Stähli *et al*., 2008; Chiaia *et al*., 2007). An example of the application of FRC with steel fibers is the hyperbolic paraboloid Oceanographic Museum in Valencia, Spain. Nevertheless, studies have reported that FRC has certain limitations, such as a scarce contribution of the fibers under compression load (Meza *et al*., 2021; Abhishek and Arabinda, 2020; Daud *et al*., 2020), low workability due to the incorporation of the fibers (Meza *et al*., 2021; Abhishek and Arabinda, 2020; Daud *et al*., 2020), and the high cost of the reinforcing elements (Meza *et al*., 2021; Meza and Siddique, 2019; Emon *et al*., 2017). As a solution to the high price of FRC, researchers have proposed using alternative and recycled fibers, aiming to reduce the cost of FRC and promote green engineering. Signorini and Volpini (2021) studied the mechanical performance of fiber-reinforced cement composites with fully recycled plastic elements. Their results showed that recycled fibers could sustain the economy of construction fields. Malek *et al*. (2020) analyzed the characteristics of recycled polypropylene fibers and reported variability in the mechanical responses of FRC using said elements. Ming *et al*. (2021) investigated the compressive behavior of recycled waste fibers in cement-based composites, concluding that steel waste fibers can provide similar mechanical properties to industrial ones.

This literature review indicates that the materials used in curve structures are plain concrete, concrete with a textile reinforcement, and concrete with conventional reinforcements. These structures are usually analyzed with finite element methods or full-scale experimentation. It is worth noting that the experimental study of FRC applied to dome-shaped structures is still a developing field that deals with topics such as the capacities of FRC in arc structures.

This research experimentally analyzed FRC in thick dome-shaped structures using seven different reinforcing elements including industrial, recycled, and alternative materials, varying the fiber doses in a total of 21 tests. This study considered 22 samples and replicated those with atypical behavior. The dome-shaped samples were tested under a central load until failure. The main objectives of this study were a) to analyze the mechanical capacities of FRC in dome-shaped structures, b) to study the effect of fiber dosage on mechanical properties, and c) to explore recycled and alternative materials as reinforcing elements in these structures. Based on these objectives, the authors aim to contribute to a better understanding of the scope and limitations of FRC with different reinforcing elements. In this study, the specimens had fibers as the only reinforcement. This technique is typical; structures typically use fibers as reinforcement elements without incorporating re-bars (*i.e.*, Oceanografic Valencia by Felix Candelas), thus reducing building times.

Material and methods

Fibers used as reinforcing elements

This study considered seven reinforcing elements, including two materials (steel and polypropylene), with diverse origins: industrial (those manufactured under a registered trademark), recycled (those obtained from discarded materials), and alternative (those generated from materials obtained in local stores). Furthermore, the fibers had different shapes, *i.e.*, end-hooked, straight, and crimped. Table 1 indicates the fiber characteristics of the reinforcing elements used.

Industrial fibers were selected because they have a higher mechanical capacity than other industrial reinforcing elements (Meza *et al*., 2014). On the other hand, recycled PET fibers were produced using waste bottles, which were cut manually to form a plastic sheet and sectioned with a guillotine to make the reinforcing elements. The PET fibers had the following dimensions: a width of 3 mm, a thickness of 0,3, and a length of 23,5 mm. The methodology followed to produce the PET fibers was similar to that of a previous study (Meza and Siddique, 2019). Moreover, alternative fibers were made from commercial wire steel (annealed and galvanized). The annealed wire had a diameter of 1,78 mm, with a composition of 0,1% carbon, 0,04% phosphorus, 0,30-0,50% magnesium, and 0,05% sulfur. The galvanized wire had a diameter of 1,2 mm and was composed of 0,07%

carbon, 0,03-0,04% phosphorus, 0,30-0,31% magnesium, 0,035-0,045% sulfur, and 0,075-0,085% silicon. The wire had a 250 kg/m^2 zinc layer.

The fibers (alternative annealed, alternative galvanized, and recycled PET) were crimped with the device shown in Figure 1, which was developed by A. Meza and the research group. The crimped device has a guide, two gears, and a crank. The two gears have a 2,5 module, with 22 teeth 3,75 mm in height and a crank to activate the crimped gears in the rear.

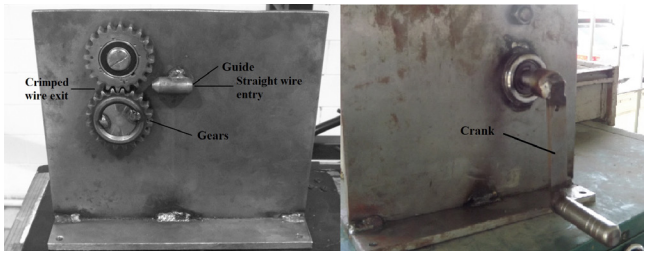

Figure 1. Front and rear view of the crimping device
Source: Authors

Table 1. Fibers used

Fiber series	Origin	Shape	Material	Aspect ratio (mm/mm)	Tensile strength (MPa)
A1	Alternative	Crimped	Annealed steel	22	340
A2	Alternative	Crimped	Galvanized steel	22	479
R1	Recycled	Straight	PET	22	250
R2	Recycled	Crimped	PET	22	250
D1	Dramix	Hooked-end	Steel	66,6	1 160
E1	Master-fiber	Straight-microfiber	Polypropylene	NA	300
E2	Tuf-strand-sf-Euclid	Straight-macrofiber	Polypropylene	74	625

The tensile strength was extracted from Meza and Shaikh (2020), Meza and Siddique (2019), and Meza *et al.* (2014).

Source: Authors

Experimental design

The concrete design consisted of ordinary Portland cement CPC 30R, in compliance with the NMX-C-414-ONNCE Mexican norm (2017) and two aggregates (fine and coarse river sand). The characteristics of these materials are as follows: i) the cement had a density of 3,15 g/cm^3; ii) the fine aggregate had a density of 2,5 g/cm^3, a fineness modulus of 2,8, and a water absorption of 3,3%; and iii) the coarse aggregate had a density of 2,68 g/cm^3, a maximum size of 20 mm (3/4 in), and a water absorption of 1,1%.

The experiments included a control and 21 fiber-reinforced concrete samples, employing seven reinforcement types and three dose levels. Samples with atypical behavior were repeated. Atypical values were evaluated using both the trends of the tested fiber-reinforced concrete and literature reports via a normalized test. Changes in the fiber aspect ratio were not evaluated because the fiber dose had a greater impact on mechanical characteristics (Meza *et al.*, 2021; Abhishek and Arabinda, 2020; Daud *et al.*, 2020; Meza and Shaikh, 2020; Chiaia *et al.*, 2019; Meza and Siddique, 2019; Meza *et al.*, 2014). There were four dome-shaped specimens with atypical behavior due to issues related to preparation or testing. Furthermore, this performance could be attributed to the random distribution of the fibers in the concrete matrix. It is essential to indicate no trend was observed in the atypical samples. Table 2 shows the proportions of the 22 different mixes used. An asterisk denotes the samples that showed atypical behavior and were repeated.

Table 2. Description of the proportions used in the experiments of this study

Specimen series	Fiber series	Fiber dose, kg/m^3	w/c ratio	Cement, kg/m^3	Fine aggregate, kg/m^3	Coarse aggregate, kg/m^3	Additive, kg/m^3	Slump, mm
C.0	---	---	0,5	383	672	1 100	10	90
A1.20	A1	20	0,5	383	672	1 100	10	50
A1.30*	A1	30	0,5	383	672	1 100	10	35
A1.40	A1	40	0,5	383	672	1 100	10	20
A2.20	A2	20	0,5	383	672	1 100	10	70
A2.30	A2	30	0,5	383	672	1 100	10	62
A2.40	A2	40	0,5	383	672	1 100	10	55
R1.2	R1	2	0,5	383	672	1 100	10	79
R1.4	R1	4	0,5	383	672	1 100	10	80
R1.6*	R1	6	0,5	383	672	1 100	10	75
R2.2	R2	2	0,5	383	672	1 100	10	65
R2.4	R2	4	0,5	383	672	1 100	10	63
R2.6	R2	6	0,5	383	672	1 100	10	60
D1.20*	D1	20	0,5	383	672	1 100	10	75
D1.30	D1	30	0,5	383	672	1 100	10	68
D1.40	D1	40	0,5	383	672	1 100	10	59
E1.2	E1	2	0,5	383	672	1 100	10	85
E1.4	E1	4	0,5	383	672	1 100	10	80
E1.6	E1	6	0,5	383	672	1 100	10	83
E2.2*	E2	2	0,5	383	672	1 100	10	80
E2.4	E2	4	0,5	383	672	1 100	10	72
E2.6	E2	6	0,5	383	672	1 100	10	68

Source: Authors

Specimen mixing, casting, and curing

First, the materials (cement, aggregates, fibers, additive, and water) were weighed under lab conditions. Second, the materials were manually stirred for up to 3 min without water. The water was added, and the materials were mixed for another 3 min to achieve homogeneity. Finally, the specimens were cast in steel molds, demolded and cured for 28 days, in accordance with ASTM C192 (ASTM International, 2017).

Mold design and testing

The process of elaborating the dome-shaped concrete specimens was based on female and male molds. The female mold controlled the outer shape of the dome sample, and

the male mold controlled the inner one. Figure 2 shows the sketch of the molds and the concrete dome element.

The demolding of the dome sample was simulated using SolidWorks software to ensure a correct extraction (Figure 3). The analysis suggested a corner rounding for the two sections (in black) located in the bottom fillets of the dome (inner and outer edges). Grey sections indicate negative and positive draft angles, implying an adequate extraction of the hardened sample. Figure 3 shows the demolding analysis results.

The mold used to create the dome-shaped samples was made of stainless steel and had a thickness of 1,21 mm (this material was workable and allowed shaping the dome mold). The mold had two parts (male and female). The female mold was sectioned into two parts, aiming to facilitate the removal of the dome specimen when it hardened. The mold also had two spacers that ensured a uniform thickness. The male mold was a single element (without a section) with the same dimensions as the inner shape of the specimen. At the bottom of the male mold was a handle that allowed extracting the hardened sample. Figure 4 shows the male and female molds.

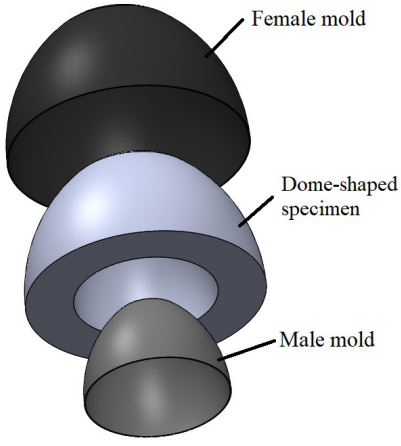

Figure 2. Sketch of the molds proposed to produce the dome-shaped specimen
Source: Authors

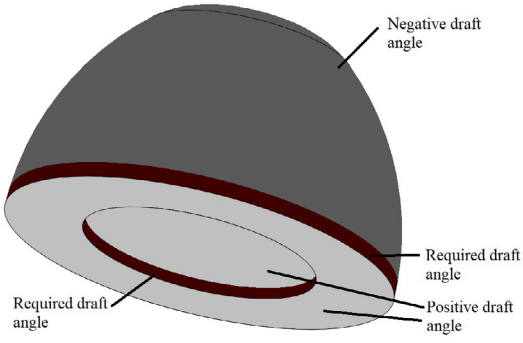

Figure 3. Dome extraction analysis using SolidWorks
Source: Authors

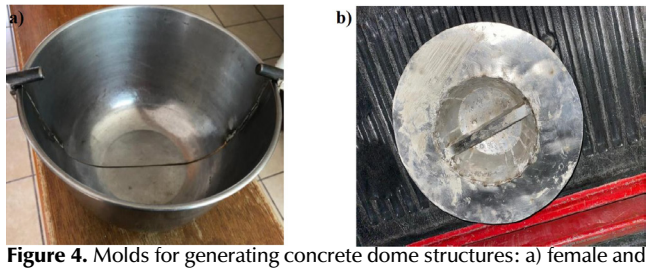

Figure 4. Molds for generating concrete dome structures: a) female and b) male
Source: Authors

The male and female molds were assembled and placed on a flat surface. The open section was facing up, and the closed one was facing down to take advantage of the force of gravity and prevent the dispersion of the material. Then, the mixture was settled into the mold, filling the third part of the sample's total volume, and it was then compacted to avoid air encapsulation. The process was repeated until the concrete covered all the mold. Compaction was performed with a flat rod 16 mm in diameter and 24 mm in length and rounded tamping ends. The rod of each layer was uniformly distributed over the cross-section of each layer with 25 strokes. Finally, the specimen was covered with a plastic sheet to reduce moisture loss. The dome-shaped sample was demolded after 48 h and cured according to the ASTM C192 (ASTM International, 2017). Figure 5 shows the procedure followed to elaborate the specimens.

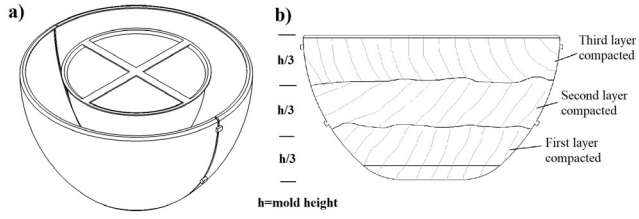

Figure 5. a) Assembly of male and female molds; b) compaction procedure
Source: Authors

Figure 6 shows the detailed geometric dimensions of the dome specimens. The demolding issues observed in the analysis were solved using 3 mm fillets. The dome-shaped elements have the following dimensions: 50 mm thickness, 150 mm height, 250 mm outer diameter, and a ratio (ratio/thickness) of 2,5. A thick shell was considered (Gere, 2009). The upper section of the dome specimen has a flat 58 mm part, where the load was applied.

A 59 kN Galdabini hydraulic machine was used during sample testing, which was controlled at 5 mm/min. The possible irregularities in the contact surface between the top of the dome specimen and the load were adjusted using a neoprene pad. The neoprene pad had a diameter of 100 mm and a thickness of 25 mm. Specimen deformation was measured via a plunger dial indicator with a measuring range of 25 mm, a resolution of 0,25 mm, and an accuracy of ±0,25 µm. The load was on the top of the structure, simulating a dead punctual load. Figure 7 shows the test setup of the dome specimen.

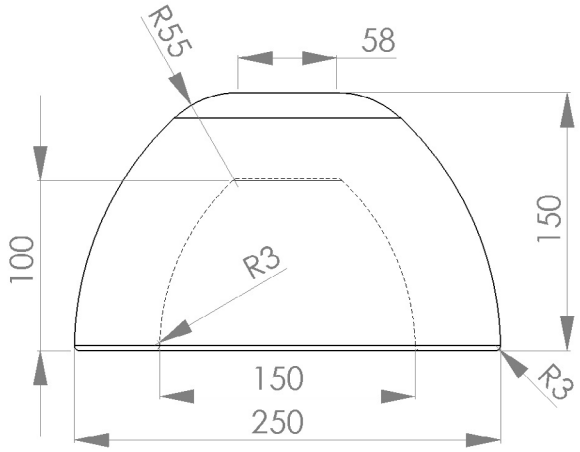

Figure 6. Geometric dimensions of the dome-shaped structure (dimensions in mm)
Source: Authors

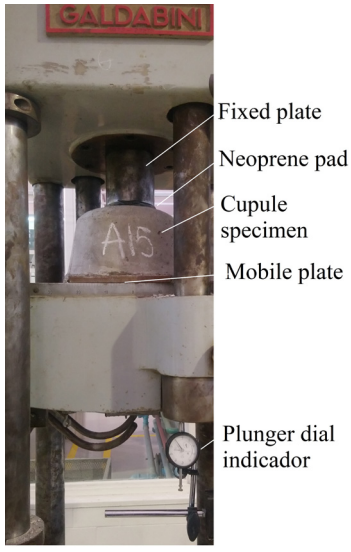

Figure 7. Test setup of the cupule specimen
Source: Authors

Results and discussion

Slump

The properties of the concrete were evaluated in the fresh state while following the standard test method for the flow of FRC through an inverted slump cone, according to ASTM C995 (ASTM International, 2018). Table 2 shows the results of the slump tests for batches with different fibers and without fibers (control). The data show a reduced workability due to the addition of the fibers, which depends on fiber material and dosage, where the minimum difference was 6% and the maximum one was 78% with respect to the control sample. The reduction in the workability of FRC is a normal phenomenon that has been reported in other studies (Meza *et al*., 2021; Meza and Siddique, 2019). The maximum and minimum slumps were found on samples with polymeric microfibers and annealed crimped fibers. The highest workability corresponded to polymeric microfibers and is attributed to the flexibility of the reinforcing elements, an effect that has also been previously reported (Meza *et al*., 2021).

On the other hand, the lowest slump, observed in concrete with annealed steel fibers, was related to the ability to trap water on the wire surface. Figure 8 shows the surface conditions of the galvanized and annealed steel wires with a 300X zoom lens. There was a higher slump on the annealed surface than on the galvanized one, with hints of corrosion pitting due to the ability to trap the humidity of the environment. This surface condition on annealed wire absorbed the moisture of the concrete mix, thus reducing workability. In contrast, the zinc layer on the surface of the galvanized wire entailed a smooth surface. Moreover, the comparison between the industrial, recycled, and alternative fibers indicated a superior slump performance for industrial vs. recycled or alternative elements. In some cases, the reduction was scarce, i.e., concrete with galvanized reinforcing elements showed a mean workability decrease of 7% with respect to Dramix elements. However, other samples exhibited a considerable slump change: the difference between Dramix and annealed fibers was 48%. Finally, the batches with polymer fibers (industrial and recycled) were similar, with a difference lower than 24%.

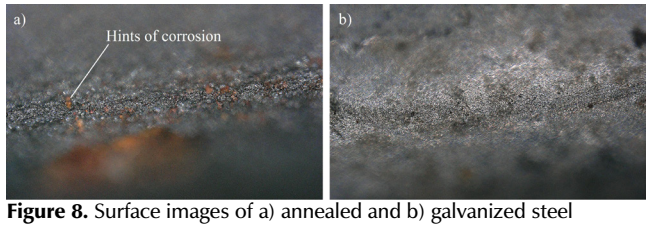

Figure 8. Surface images of a) annealed and b) galvanized steel
Source: Authors

Dome-shaped samples

Load deflection

Figure 9 presents the load displacement curves for the tested samples. These curves show that the dome-shaped structures, with or without fibers, started with an elastoplastic behavior, followed by a nonlinear load-displacement relation, with different strength and deformation ranges, attributed to the incorporation of the reinforcing elements, the dose, and efficiency. The following sections analyze aspects such as stiffness, peak load, the ductility index, and toughness.

Stiffness

Equation (1) shows the relation used to calculate the relative stiffness, which is based on the NMX-C-128-ONNCCE norm (2013) and was adapted to this study. Table 3 shows the stiffness results, with the data indicating that all the fiber-reinforced dome-shaped structures had a higher initial stiffness than the control specimen. However, it must be pointed out that the change in fiber dose had a low contribution to stiffness, with a maximum difference of 22%.

The highest stiffness values were found for dome-shaped steel FRC. Annealed samples had the best performance, which can be attributed to their rough surface and larger cross-section in comparison with the other steel fibers tested. Regarding stiffness, the samples with annealed fibers were followed by those with industrial and galvanized steel ones. On the other hand, the samples with polypropylene fibers showed a lower stiffness than those with steel fibers, which can be attributed to their high flexibility and ductility (Meza *et al*., 2021). The lowest values were reported by samples with straight PET fibers, exhibiting a higher stiffness (7%) with respect to the control.

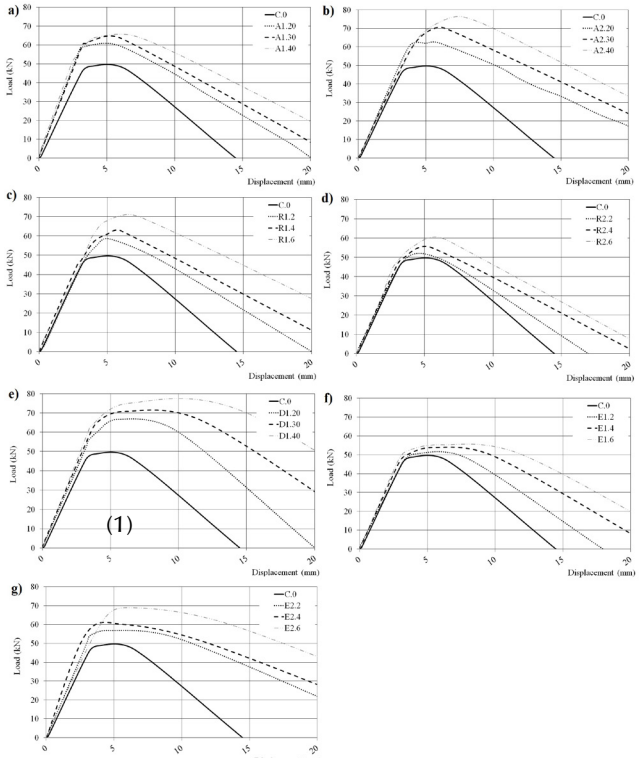

Figure 9. Load-deflection curves of dome-shaped concrete samples reinforced with a) annealed crimped steel fibers, b) galvanized crimped steel fibers, c) straight PET fibers, d) crimped PET fibers, e) industrial hooked-end steel fibers, f) straight polymeric microfibers, and g) straight polymeric macro fibers
Source: Authors

$$S_o = \frac{L_o^{40\%} - L_o^{0,00005}}{\delta_o^{40\%} - \delta_o^{0,00005}} \quad (1)$$

where S_o is the stiffness, $L_o^{40\%}$ is the load corresponding to 40% of the ultimate value, $L_o^{0,00005}$ is the load corresponding to 0,00005 of the ultimate value, $\delta_o^{40\%}$ is the displacement corresponding to 40% of the ultimate value, and $\delta_o^{0,00005}$ is the displacement corresponding to 0,00005 of the ultimate value

Peak load

Table 3 shows the peak load results for samples with and without fibers. The data indicate that the peak load capacity increases by incorporating reinforcing elements into the concrete. In fact, all the specimens with fibers exhibited a superior performance when compared to the control. The highest difference was 54% for the sample with galvanized crimped steel fibers and a fiber dose of 40 kg/m^3, while the lowest difference was reported by a dose of 2 kg/m^3 of industrial polymeric microfibers, with a maximum difference of 4% regarding the control sample. On the other hand, the mean responses of the samples with fibers indicated the superior performance of dome-shaped specimens with steel elements, followed by those with polymer reinforcements. Moreover, changing the fiber dose had a low effect on the maximum load (lower than 23%).

Table 3. Mechanical behavior of the dome-shaped specimens

ID	Stiffness, MN/m	Peak load, kN	Ductility index, mm/mm	Toughness, J
C.0	14,13	48,8	1,2	411,2
A1.20	19,06	60,3	1,8	710,4
A1.30	18,5	63,8	2,3	787,5
A1.40	20,15	65,0	2,8	952,3
A2.20	16,06	62,4	2,1	841,7
A2.30	15,02	70,7	2,6	990,8
A2.40	14,99	76,5	3,2	1 218,8
R1.2	14,2	58,6	1,6	635,8
R1.4	16,11	62,7	2,0	774,5
R1.6	14,99	70,0	2,1	1 066,2
R2.2	14,91	52,0	1,5	493,2
R2.4	15,54	55,1	1,8	609,7
R2.6	15,6	60,5	2,2	731,1
D1.20	16,3	66,7	1,7	795,2
D1.30	17,06	70,8	1,9	1 121,7
D1.40	17,98	75,0	2,0	1 486,3
E1.2	14,41	50,5	1,3	546,4
E1.4	15,75	53,9	1,9	723,5
E1.6	16,46	55,3	2,1	869,9
E2.2	16,71	56,9	1,5	889,2
E2.4	18,78	60,0	2,0	1 026,5
E2.6	14,95	68,9	2,3	1 389,5

Source: Authors

Ductility index

Nehdi *et al*. (2015) proposed calculating the ductility index by dividing the displacement at peak load by the corresponding cracking load. The researcher uses the peak load as a reference because concrete's mechanical performance resembles that of a fragile material. Thus, it is more feasible to localize the peak load than the yield displacement. Table 3 shows the results of this ratio applied to FRC dome-shaped samples. The data indicate that the FRC specimens have a higher ductility index than the control. The maximum and minimum differences are found for crimped steel fibers and

industrial polymeric microfibers, with doses of 40 and 2 kg/m^3, respectively. The differences reach 2,2 and 1,4 times the control sample's capacity. These results also prove that increasing the fiber dose enhances the ductility index of dome-shaped structures by up to 61%. The mean data show that polymeric fibers have a better ductility index than steel ones. This behavior was contrary to that of the stiffness and peak load. In comparison with the data reported by Nehdi *et al*. (2015), the range of the ductility index in FRC dome-shaped structures was similar to that of FRC tunnel structures.

Toughness

Table 3 shows the toughness of the dome-shaped samples, which was measured through the energy calculated based on the area under the load-displacement curve until failure. The data indicate that the toughness of the dome-shaped samples depends on the characteristics of the reinforcement, i.e., all the fiber-reinforced specimens exhibited a better energy absorption than the control, with a difference that increased with the fiber amount. The highest toughness was reported by the specimen with industrial polymeric macrofibers at a dose of 6 kg/m^3, with a difference of 3,6 times the capacity of the control sample. In contrast, the lowest difference corresponded to the specimen with crimped PET fibers at a dose of 2 kg/m^3, with a superior toughness of 20% regarding the control. Moreover, the data reported the best toughness values for dome-shaped elements with industrial fibers (steel and polymeric macrofibers), followed by samples with alternative and recycled ones. Nehdi *et al*. (2015) reported that the increase in the toughness of concrete tunnel specimens reinforced with steel fibers amounts to 95% compared to control samples. In this study, some FRC dome-shaped samples exceed the records presented by Nehdi *et al*. (2015), thus proving the contribution of fibers to dome elements.

FEM study

The failure mode of the dome structure was studied using the finite element method (FEM). The aim was to study the stress gradients and the area where the cracks couldstart up. Only linear properties were considered. The FEM study was static, using a first-order tetra mesh with four Jacobian points, a maximum element size of 17,7 mm, and a total of nodes and elements of 11 367 and 7 223, respectively. The concrete properties were isotropic linear elastic, with a modulus of elasticity of 13 GPa, a Poisson ratio of 0,2, and a density of 2 400 kg/m^3 (based on the data indicated by Meza *et al*. in 2021). The movement of the dome structure was constrained in its low section in the z-axis (perpendicular to the load direction). The other axes (x-y) were not constrained, simulating the conditions of the tests. The load was applied in a perpendicular direction (15 kN) onto the superior face of the dome structure, with a diameter of 58 mm. Figure 10 shows the FEM results, where the maximum stress was observed in the upper and lower corners of the dome sections, corresponding to the load application and holder areas. During the test, the failure started in the top section, where the stress was higher, and moved to the opposite zone. Moreover, the dome samples with high fiber contents demonstrated a higher formation of microcracks than those without fibers or with low proportions. However, the fibers delayed crack propagation in the dome specimens, enhancing the rate of load recovery after cracking. Bhosale *et al*. (2020) and Adel *et al*. (2021) studied the crack behavior of concrete structures, indicating a similar performance (the fibers controlled crack propagation but were more susceptible to a high number of micro-cracks). This phenomenon was attributed to the presence of air in the interface of the concrete fiber.

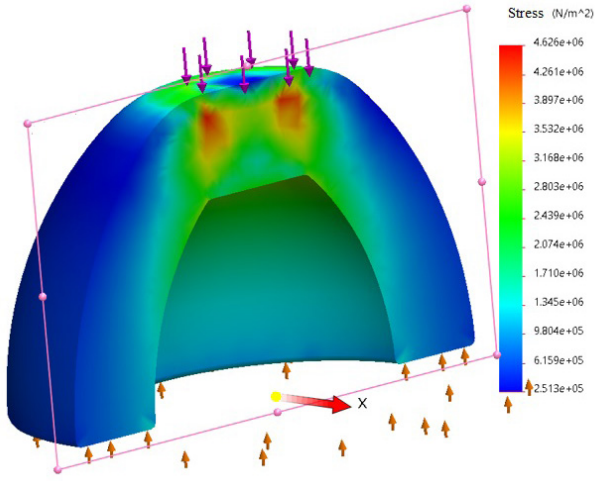

Figure 10. a) FEM study of the dome-shaped sample; b) cracking of the dome-shaped sample
Source: Authors

Cracking behavior

All the dome-shaped samples exhibited a progressive failure, including those without fibers. This effect was attributed to the arc shape of the specimens, which maintained the load after the first crack and gradually declined. Figure 11 shows the procedure observed during the cracking of the dome-shaped specimens, which had three stages. Stage I was characterized by an elastoplastic behavior, observed with a semi-linear behavior in the load-displacement graph. Stage II showed a nonlinear load-displacement relation, reaching the maximum load zone. Stage III corresponded to a decreasing segment in the load-defection curve, which depended on the ductility behavior of the dome structure until the failure point. The range of strength and deformation is different in each part of the graphs, which can attributed to the incorporation of fibers, their dose, and their efficiency.

Fiber efficiency

Equation (2) shows the relation used to calculate the fiber efficiency, which compares the capacity of the FRC dome-shaped structure against that of the control sample. Moreover, the Equation considers the fiber dose incorporated into the mix. Figure 12 shows the results obtained for the fiber

efficiency, in correspondence with the peak load, ductility index, and toughness. Since the fiber dose depends on the density of the fiber materials, the analysis is depicted in two groups (steel and polymeric FRC samples).

$$\eta_f = \frac{\varphi_f - \varphi_c}{\varphi_f D_f} \quad (2)$$

where η_f is the fiber efficiency, φ_f is the capacity of the dome-shaped structure reinforced with fibers, φ_c is the capacity of the control dome-shaped structure, and D_f is the fiber dose.

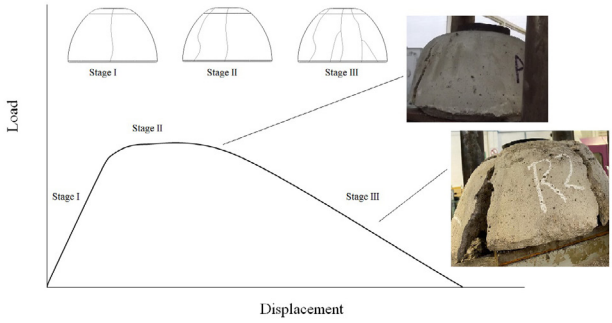

Figure 11. Cracking process of the dome-shaped samples, general performance
Source: Authors

Figure 12. Fiber efficiency of dome-shaped samples: a) peak load, b) ductility index, and c) toughness

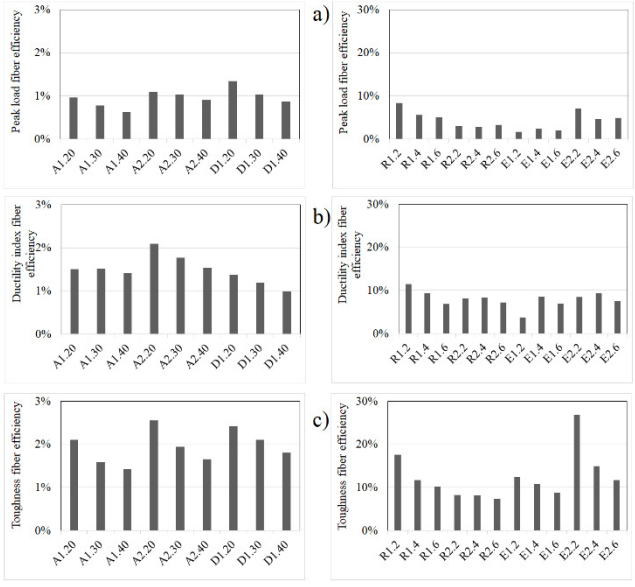

Source: Authors

Fiber efficiency and peak load

Figure 12a shows the results obtained for the fiber efficiency regarding the peak load of dome samples. The data indicate that steel FRC with annealed, galvanized, and industrial elements and a low fiber dose is more effective than that with a high proportion of reinforcing elements. Furthermore, the dome-shaped samples with straight PET fibers and industrial polymeric macrofibers showed a similar trend to elements with steel fibers (the specimens with a low fiber content had high efficiency). This phenomenon was attributed to i) the nonlinear increase in the peak load, which was not proportional to the fiber dose; and ii) the fact that the mechanical strength of the fiber was higher than its adherence to the concrete. This result agreed with other studies, which indicate that the fiber material has a greater influence than the adherence between the fiber and the concrete (Meza and Shaikh, 2020; Meza *et al.*, 2004; Poveda *et al.*, 2020; Qi *et al.*, 2018; Breitenbücher *et al.*, 2014). On the other hand, the data show that dome-shaped specimens with industrial reinforcements have the best efficiency, followed by those with galvanized and annealed ones. In contrast, the samples with polymeric fibers show the best behavior with recycled, straight elements, followed by those with industrial polymeric macrofibers, recycled crimped PET, and industrial polypropylene microfibers.

Fiber efficiency and ductility

Figure 12b shows the results regarding fiber efficiency and ductility. The overall results indicate that dome-shaped elements reinforced with straight PET and with crimped annealed fibers perform better than the other fibers tested. Moreover, the data prove that samples reinforced with high steel fiber contents have reduced efficiency, i.e., the lowest efficiency was reported by samples A1.40, A2.40, and D1.40. In contrast, samples with polymeric reinforcement show no trend with respect to fiber efficiency. Meanwhile, the elements with straight PET fibers exhibit a similar behavior to those with steel ones (the best efficiency reported for samples with low fiber contents), and the other dome samples show different performances. Specimens with crimped PET fibers, industrial polymeric macrofibers, and polymeric microfibers show the best efficiency at a central dose (4 kg/m^3).

Fiber efficiency in the toughness

The data show better efficiencies in dome-shaped samples with a low proportion of reinforcing elements. The global results indicate that the specimens with alternative annealed and industrial fibers perform better than those with galvanized ones. This was attributed to the mechanical properties of the fibers, i.e., the deformation capacity of annealed steel and the strength of industrial steel fibers (Ming *et al.*, 2021; Meza *et al.*, 2014). On the other hand, the specimens with polymeric industrial macrofibers showed the best efficiency, followed by those with recycled straight PET fibers, industrial microfibers, and recycled crimped PET fibers. These results are similar to those of previous studies, which point out that macrofibers and recycled PET have adequate adherence to concrete and tensional strength (Ming *et al.*, 2021; Meza *et al.*, 2021). Figure 12c shows the fiber efficiency results regarding the dome samples' toughness.

Conclusions

The experimental results obtained for the dome-shaped samples show the load-displacement curves to have different ranges of strength and deformation, which is attributed to the incorporation of fibers, their dose, and their efficiency, with higher mechanical performances than the control. Each fiber type showed both advantages and limitations in the different stages of this research, as is presented below.

I: The data showed a reduced workability due to the addition of fibers, which was higher on FRC with annealed elements (78% regarding the control) and is attributed to the ability to trap water on its surface.

II: The FEM study located the maximum stress at the edges of the load and the holder sections of the dome-shaped specimen, where the cracks start up and grow.

III: The samples with high fiber contents showed a larger number of microcracks than the control and those with a low fiber proportion. However, the reinforcing elements controlled the cracks and increased the ductility of the structural elements.

IV: The fiber efficiency study pointed out that samples with a low fiber content (20 and 2 kg/m^3) had a higher mechanical efficiency than those with a high proportion (40 and 6 kg/m^3).

V: The dome shape maintained the load after the first crack and declined gradually according to the reinforcement capacity, highlighting the mechanical performance of industrial hooked steel fibers, alternative crimped annealed fibers, alternative crimped galvanized fibers, industrial polymeric macrofibers, and recycled straight PET fibers.

Acknowledgments

The authors wish to acknowledge Tecnológico Nacional de México and IT Aguascalientes for the support provided to this research and the access granted to the laboratory for testing composite materials. Moreover, the authors wish to thank ME Rodolfo B. Sierra Ortiz, Eng. Fernando Chavez Valdivia, and Eng. Rafael Reyes Cortés for participating in this study.

CRediT author statement

Alejandro Meza de Luna: conceptualization, data curation, formal analysis, funding acquisition, investigation, methodology, project administration, resources, software, supervision, validation, visualization, writing (original draft, review, and editing).

Elia M. Alonso and Adrián Bonilla: conceptualization, investigation, methodology, supervision, validation, visualization, writing (review and editing).

Conflicts of interest

The authors declare that no known financial interest or relationship could have influenced the work reported in this paper.

References

Abbood, I. S., Odda, S. A., Hasan, K. F., and Jasim, M. A. (2020). Properties evaluation of fiber reinforced polymers and their constituent materials used in structures – A review. *Materials Today: Proceedings, 43*(2), 1003-1008.

Abhishek, J., and Arabinda, S. (2020). Experimental study on the properties of steel fibre reinforced concrete. *Indian Journal of Engineering, 17*(47), 151-162.

Adel, M., Matsumoto, K., and Nagai, K. (2021). Crack-bridging degradation and evolution in SFRC structural beams under variable amplitude flexural cyclic loading. *Computers and Structures, 272*, 114176. https://doi.org/10.1016/j.compstruct.2021.114176

ASTM International (2017). *ASTM C192: Standard practice for making and curing concrete test specimens in the laboratory*. ASTM International.

ASTM International (2018). *ASTM C39/C39M: Standard test method for compressive strength of cylindrical concrete specimens*. ASTM International.

ASTM International (2018). ASTM C78/C78M Standard test method for flexural strength of concrete (using simple beam with third-point loading). ASTM International.

ASTM International (2018). *ASTM C995-01: Standard test method for time of flow of fiber-reinforced concrete through inverted slump cone*. ASTM International.

Berger, J., Gericke, O., Feix, J., and Sobek, W. (2020). Actively bent concrete shells. *Structural Concrete, 1*(11), 2282-2292. https://doi.org/10.1002/suco.201900505

Berger, J., Gericke, O., Feix, J., and Sobek, W. (2020). Experimental investigations on actively bent concrete shells. *Structural Concrete, 21*(6), 2268-2281. https://doi.org/10.1002/suco.202000045

Bhosale, A. B., and Prakash, S. S. (2020). Crack propagation analysis of synthetic *vs.* steel *vs.* hybrid fibre-reinforced concrete beams using digital image correlation technique. *International Journal of Concrete Structures and Materials, 14*, 57. https://doi.org/10.1186/s40069-020-00427-8

Breitenbücher, R., Meschke, G., Song, F., and Zhan, Y. (2014). Experimental, analytical and numerical analysis of the pullout behaviour of steel fibres considering different fibre types, inclinations and concrete strengths. *Structural Concrete, 15*(2), 126-135. https://doi.org/10.1002/suco.201300058

Cadoni, E., Meda, A., and Plizzari, G.A. (2009). Tensile behaviour of FRC under high strain-rate. *Materials and Structures, 42*, 1283-1294. https://doi.org/10.1617/s11527-009-9527-6

Caycedo, M. S., Siqueira, G. H., Vieira, L. C. M., and Vizotto, I. (2019). Evaluation of structural capacity of triangular and hexagonal reinforced concrete free-form shells. *Engineering Structures, 188*, 519-537. https://doi.org/10.1016/j.engstruct.2019.03.044

Chiaia, B., Fantilli, A. P., and Vallini, P. (2007). Evaluation of minimum reinforcement ratio in FRC members and application to tunnel linings. *Materials and Structures, 40*, 593-604. https://doi.org/10.1617/s11527-006-9166-0

Chiaia, B., Fantilli, A. P., and Vallini P. (2009). Evaluation of crack width in FRC structures and application to tunnel linings. *Materials and Structures, 42*, 339. https://doi.org/10.1617/s11527-008-9385-7

Chun, N. H. (2005). Ultimate strength of large scale reinforced concrete thin shell structures. *Thin Walled Structures, 43*, 1418-144.

Cocchetti, G., Colasante, G., and Rizzi, E. (2011). On the analysis of minimum thickness in circular masonry arches. *Applied Mechanics Reviews, 64*(5), 050802. https://doi.org/10.1115/1.4007417

Daud, R. A., Daud, S. A., and Al-Azzawi, A. A. (2020). Tension stiffening evaluation of steel fibre concrete beams with smooth and deformed reinforcement. *Journal of King Saud University, 33*(3), 147-152. http://doi.org/10.1016/j.jksues.2020.03.002

Du, W., Liu, Q., Zhou, Z., Uddin, N. (2019). Experimental investigation of innovative composite folded thin cylindrical concrete shell structures. Thin-Walled Structures, 137 (2019), 224–230. https://doi.org/10.1016/j.tws.2019.01.014

Emon, M. A. B., Manzur, T., and Sharif, M. S. (2017). Suitability of locally manufactured galvanized iron (GI) wire fiber as reinforcing fiber in brick chip concrete. *Case Studies in Construction Materials, 7*, 217-227. https://doi.org/10.1016/j.cscm.2017.08.003

Gere, M. J. and Barry, J. G. (2009). *Mechanics of materials* (7th ed.). Cengage Learing.

Gomes, C., Parente, M., Azenha, M., and Lino, J.C. (2018). An integrated framework for multi-criteria optimization of thin concrete shells at early design stages. Advanced Engineering Informatics, 38, 330–342. https://doi.org/10.1016/j.aei.2018.08.003

Małek, M., Jackowski, M., Łasica, W., and Kadela, M. (2020). Characteristics of recycled polypropylene fibers as an addition to concrete fabrication based on Portland cement. *Materials, 13*(8), 1827. https://doi.org/10.3390/ma13081827

Meza, A., Ortiz, J. A., Peralta, L., Pacheco, J., Soto, J. J., Rangel, S. H., Padilla, R., and Alvarado, J. (2014). Experimental mechanical characterization of steel and polypropylene fiber reinforced concrete. *Revista Técnica Facultad de Ingeniería Universidad de Zulia, 37*(2), 106–115.

Meza, A., Pujadas, P., Meza, L. M., Pardo-Bosch, F., and López-Carreño, R. D. (2021). mechanical optimization of concrete with recycled PET fibres based on a statistical-experimental study. *Materials, 14*(2), 240. https://doi.org/10.3390/ma14020240

Meza, A. and Shaikh, F. U. A. (2020). Anisotropy and bond behaviour of recycled polyethylene terephthalate (PET) fibre as concrete reinforcement. *Construction and Building Materials, 265*, 120331. https://doi.org/10.1016/j.conbuildmat.2020.120331

Meza, A., and Siddique, S. (2019). Effect of aspect ratio and dosage on the flexural response of FRC with recycled fiber. *Construction and Building Materials, 213*, 286-291. https://doi.org/10.1016/j.conbuildmat.2019.04.081

Ming, Y., Chen, P., Li, L., Gan, G., and Pan, G. (2021). A comprehensive review on the utilization of recycled waste fibers in cement-based composites. *Materials, 14*(13), 3643. https://doi.org/doi.org/10.3390/ma14133643

Nehdi, M. L., Abbas, S., and Soliman, A. M. (2015). Exploratory study of ultra-high performance fiber reinforced concrete tunnel lining segments with varying steel fiber lengths and dosages. *Engineering Structures, 101*, 733-742. https://doi.org/10.1016/j.engstruct.2015.07.012

NMX-C-128-ONNCCE (2013). *Determination of modulus of elasticity and Poisson ratio*. https://www.dof.gob.mx/nota_detalle.php?codigo=5577342&fecha=31/10/2019#gsc.tab=0

NMX-C-414-ONNCCE (2017). *Construction industry-hydraulic cementants-specifications and test methods*. https://www.onncce.org.mx/es/venta-normas/fichas-tecnicas?view=item&id=1879

Pereira, M. (2022, September 10). Cáscaras de hormigón: principios de diseño y ejemplos construidos. *Arch Daily*. https://www.archdaily.mx/mx/895405/cascaras-de-hormigon-principios-de-diseno-y-ejemplos-construidos

Poveda, E., Yu, R. C., Tarifa, M., Ruiz, G., Cunha, V. M. C. F., and Barros, J. A. O. (2020). Rate effect in inclined fibre pullout for smooth and hooked-end fibres: A numerical study. *International Journal of Fracture, 223*, 135-149. https://doi.org/10.1007/s10704-019-00404-7

Qi, J., Wu, Z., Zhongguo, J.M., and Wang, J. (2018). Pullout behavior of straight and hooked-end steel fibers in UHPC matrix with various embedded angles. *Construction and Building Materials, 191*, 764-774. https://doi.org/10.1016/j.conbuildmat.2018.10.067

Sharei, E., Scholzen, A., Hegger, J., and Chudoba, R. (2017). Structural behavior of a lightweight, textile-reinforced concrete barrel vault shell. *Composite Structures, 171*, 505-514. https://doi.org/10.1016/j.compstruct.2017.03.069

Signorini, C., and Volpini, V.D. (2021). Mechanical performance of fiber reinforced cement composites including fully-recycled plastic fibers. *Fibers, 9*(3), 16. https://doi.org/10.3390/fib9030016

Stähli, P., Custer, R., and Van-Mier, J. G. M. (2008). On flow properties, fibre distribution, fibre orientation and flexural behaviour of FRC. *Materials and Structures, 41*, 189-196. https://doi.org/10.1617/s11527-007-9229-x

Tamayo, J. L. P., Morsch, I. B., and Awruch, A. M. (2013). Static and dynamic analysis of reinforced concrete shells. *Latin American Journal of Solids and Structures, 10*, 1109-1134.

Tomás, A., and Martí, P. (2010). Shape and size optimisation of concrete shells. *Engineering Structures, 32*(6), 1650-1658. https://doi.org/10.1016/j.engstruct.2010.02.013

Verwimp, E., Tysmans, T., Mollaert, M., and Wozniak, M. (2016). Prediction of the buckling behavior of thin cement composite shells: Parameter study. *Thin Walled Structures, 108*, 20-29. https://doi.org/10.1016/j.tws.2016.07.011

Wenfeng, D., Qi, L., Zhiyong, Z., and Nasim, U. (2019). Experimental investigation of innovative composite folded thin cylindrical concrete shell structures. *Thin Walled Structures, 137*, 224-230. https://doi.org/10.1016/j.tws.2019.01.014

Zingoni, A., Mudenda, K., French, V., and Mokhothu, B. (2013). Buckling strength of thin-shell concrete arch dams. *Thin Walled Structures, 64*, 94-102. https://doi.org/10.1016/j.tws.2012.12.001